UC Davis
UC Davis Previously Published Works

Title

27 Al MQMAS of the δ-Al 13 -Keggin

Permalink

https://escholarship.org/uc/item/9d91960t

Journal

Dalton Transactions, 46(7)

ISSN

1477-9226

Authors

Pilgrim, CD
Callahan, JR
Colla, CA
et al.

Publication Date

2017-02-14

DOI

10.1039/c6dt04263e

Peer reviewed

CrossMark
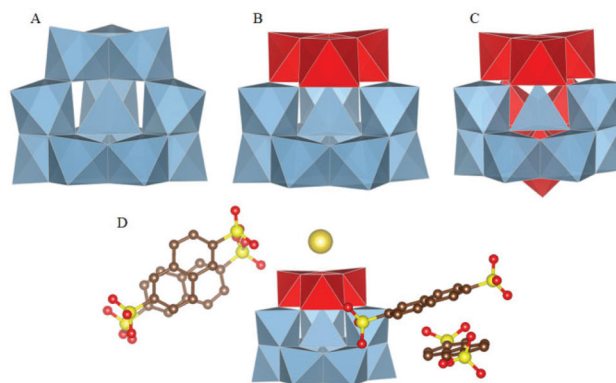← click for updates

^{27}Al MQMAS of the δ-Al$_{13}$-Keggin†

C. D. Pilgrim,‡[a] J. R. Callahan,‡[a] C. A. Colla,[b] C. A. Ohlin,[c] H. E. Mason[d] and W. H. Casey*[a,b]

One-dimensional ^{27}Al, ^{23}Na Magic-Angle-Spinning (MAS) NMR and ^{27}Al Multiple-Quantum Magic-Angle-Spinning NMR (MQMAS) measurements are reported for the δ-isomer of the Al$_{13}$ Keggin structure at high spinning speed and 14.1 T field. Values for the C_Q and η parameters are on the same scale as those seen in other isomers of the Al$_{13}$ structure. Density functional theory (DFT) calculations are performed for comparison to the experimental fits using the B3PW91/6-31+G* and PBE0/6-31+G* levels of theory, with the Polarizable Continuum Model (PCM).

Introduction

Aluminum is one of the most abundant elements, and the second most abundant metal, in the Earth's crust.[1,2] Aluminum can be found in over 200 oxide minerals and is mined for practical use—it is a lightweight building material, it can provide strong protective coatings, and aluminum oxide is even present in personal care products.[3–5] Aluminum has a high affinity for oxygen and the hydrolysis chemistry of the metal has been studied extensively in the past 60 years, yielding new polyoxometalate structures.[6–9] Of these structures, the Al$_{13}$ family of polycations is particularly interesting due to its potential presence in natural waters.[10–13]

Johansson crystallized the first known Al$_{13}$ cluster in 1960, which had the formula of $[AlO_4Al_{12}(OH)_{24}(H_2O)_{12}]^{7+}$ and formed as an ε–isomer of the ε-Baker–Figgis–Keggin structures.[8,14,15] There are potentially five isomers (α, β, γ, δ, and ε) in this series of structures and they differ by a rotation of each of the trimeric caps by 60°. The Johansson discovery, here denoted as ε-Al$_{13}$, contains a central tetrahedral AlO$_4$ unit surrounded by four trimeric Al$_3$(OH)$_6$ groups in an edge-sharing arrangement (Fig. 1A). Until recently, only the ε- and α-isomers of the structures were known to exist, with the α-Al$_{13}$ unit found in the mineral zunyite.[16,17] For several decades the ε-Al$_{13}$ isomer was the only member of this series known to exist as an ion in solution, although other ions were suspected.[18] Recently, the δ-Al$_{13}$ (Fig. 1B) was isolated from solution as the

[a]*Department of Chemistry, University of California-Davis, Davis, CA, USA*
[b]*Department of Earth and Planetary Sciences, University of California-Davis, Davis, CA, USA. E-mail: whcasey@ucdavis.edu*
[c]*Department of Chemistry, Umeå University, Umeå, Sweden*
[d]*Lawrence Livermore National Laboratory, Livermore, CA, USA*
†Electronic supplementary information (ESI) available. See DOI: 10.1039/c6dt04263e
‡These authors contributed equally to the following work.

Fig. 1 (A) The ε-Al$_{13}$-Keggin isomer is shown with blue polyhedral for the edge-shared AlO$_6$. (B) The δ-Al$_{13}$ isomer is shown with the rotated trimeric cap in red. (C) The γ-Al$_{13}$ isomer is shown with two rotated trimeric caps in red. (D) The δ-Al$_{13}$ isomer is shown with capping Na$^+$ and surrounding NDS, from Abeysinghe *et al.*[20]

sulfate salt.[18,19] However, the rotated trimeric subunit is capped by a sodium ion, which distinguishes it from the ε-Al$_{13}$ and all other isomers. The δ-Al$_{13}$ has since been synthesized in higher yield with 2,6-napthalene-disulfonate as the counter ion (Fig. 1D).[20] The γ-Al$_{13}$ isomer has recently been identified in glycine-bearing solution and has been isolated in the solid-state (Fig. 1C).[21]

Nuclear Magnetic Resonance (NMR) has proven to be a useful method for characterizing these polycations. The ^{27}Al nucleus is 100% abundant, the gyromagnetic ratio of the nucleus is sufficiently large to allow for easy detection, and the chemical-shift range is sufficiently broad to show differences between AlO$_4$, AlO$_5$, and AlO$_6$ bonding sites.[22] Solution-state data for the δ-Al$_{13}$ ion are available, as well as one-dimensional Magic Angle Spinning (1D MAS) for the solids. However, a more complete solid-state analysis has yet to be done and

would complement existing work on the ε-Al$_{13}$ and the γ-Al$_{13}$ clusters.[23,24] Due to the quadrupolar nature of the ^{27}Al isotope (nuclear spin quantum number of I = 5/2), broad asymmetric resonances are expected for regions of the solid-state spectrum that typically correspond to the AlO$_4$ and AlO$_6$ coordination environments. This broadening complicates the interpretation of the spectra.

To overcome this broadening, we here report multiple-quantum magic-angle spinning (MQMAS) NMR of the δ-Al$_{13}$. Conventional 1D MAS averages out the first-order quadrupolar interactions, but is insufficient to eliminate second-order quadrupolar broadening. The MQMAS spectra remove these second-order quadrupolar couplings. The sequence proceeds by applying a high-power pulse to excite the multiple-quantum coherences. The triple-quantum, 3Q, coherence is selectively transferred to the central transition *via* phase cycling where it is then refocused along the *z*-axis using another high-power pulse. A lower-power pulse is applied to excite the central transition and extract the isotropic echoes.[25–27] The three-pulse version of the MQMAS experiment was used, with a *z*-filter, and a decoupling scheme during acquisition. The result of this procedure is a two-dimensional (2D) NMR experiment where the isotropic projections of the different chemical sites are on the vertical (F1) axis and the original 1D spectrum is on the horizontal (F2) axis. Correlation between the two projections provides information about the number of isotropic peaks that are hidden in otherwise complicated experimental data. Different sites can be identified and be fit to yield the quadrupolar-coupling parameter, C_Q (MHz), and the dimensionless asymmetry parameter, $η$, which reflects the site symmetry. This technique can be used on any nuclei with a nuclear spin quantum number I = n/2, and can excite higher-order transitions, but is most sensitive when applied to the 3Q transition.

The experiments can be complemented with computer simulations that calculate electronic structures and that estimate the electric-field gradients (EFGs) of the nuclei in the molecules. The EFGs are important to interpret and evaluate the fits of the solid-state NMR data, as:

$$C_Q = \frac{eQV_{zz}}{h} \tag{1}$$

$$η = \frac{|V_{xx} - V_{yy}|}{V_{zz}} \tag{2}$$

where e is the elementary charge of the electron, h is Planck's constant, Q is the nuclear quadrupole moment, V_{zz}, V_{xx}, and V_{yy} are the eigenvalues of the calculated EFGs.[28–30] Values of C_Q for the octahedral sites in the ε-Al$_{13}$ and γ-Al$_{13}$ are on the order of 10 MHz for the ε-Al$_{13}$ and 6–7.5 MHz for the γ-Al$_{13}$.[23,24,31]

In this work, crystals containing the δ-Al$_{13}$ Keggin ion are characterized in the solid-state using both 1D ^{27}Al and ^{23}Na MAS, as well as 2D ^{27}Al MQMAS experiments. Crystallographic data are used in DFT calculations to help understand the nature of bonding within the AlO$_4$ and AlO$_6$ coordination environments. The calculations also yield estimates of the EFGs that can be compared to the experimental NMR data.

Experimental

Synthesis of Na(AlO$_4$Al$_{12}$(OH)$_{24}$(H$_2$O)$_{12}$)(2,6NDS)$_4$(H$_2$O)$_{13.5}$

Crystalline δ-Al$_{13}$ was prepared using a half-scale replication of the technique reported by Abeysinghe *et al*. 30 mL of 0.25 M NaOH was added dropwise to 12.5 mL of 0.25 M AlCl$_3$ solution heated to 80 °C in order to reach a hydrolysis ratio (OH$^-$/Al(III)) of 2.4. The mixture was allowed to cool to room temperature and 10 mL were loaded into a Teflon-lined Parr reaction vessel. The sample was then heated at 80 °C for 24 hours before it was removed, split into two 5 mL aliquots, placed into a pair of 20 mL glass scintillation vials, and again allowed to cool to room temperature. An aliquot of 3 mL of 0.1 M 2,6-naptha-lene-disulfonate solution was then added to each vial, causing colloidal flocculants to form immediately. These samples were allowed to stand for eight days, during which large, white, dendritic crystals formed. The crystals were extracted from the supernatant solution by vacuum filtration and submitted for X-ray crystallography and solid-state NMR analysis.

To assess the effects of heating during spinning of an NMR sample, which could potentially cause dehydration, vacuum-dried crystals were placed in a fresh glass scintillation vial and heated at 60 °C in an oven for 118 hours. The heated crystals were then removed, cooled to room temperature, and analyzed by single-crystal X-ray diffraction. No change in the δ-Al$_{13}$ structure was observed. Crystals from this treatment were then used for subsequent ^{27}Al MAS, MQMAS, and ^{23}Na MAS NMR studies.

NMR

^{27}Al and ^{23}Na NMR experiments were conducted using a 14.1T Bruker Avance 600 system equipped with a 1.3 mm MAS probe and tuned to 156.35 and 158.72 MHz, respectively. The ^{27}Al spectra were externally referenced using the ε-Al$_{13}$ solid, with the sharp AlO$_4$ peak set to $δ$ = 62.5 ppm, while the ^{23}Na spectrum was externally referenced to a static aqueous solution of NaCl, with the single peak set to $δ$ = 0.0 ppm. Samples were loaded into a zirconia ceramic rotor with Vespel® caps and were spun at $ν_R$ = 50 kHz. Frictional heating from spinning caused the sample temperature to raise to approximately 50 °C. Temperatures were calibrated by ^{207}Pb NMR of an external sample of Pb(NO$_3$)$_2$.[32] All spectra were decoupled from ^{1}H using low-power XiX decoupling[33] with a pulse width of 57 μs. For the 1D MAS experiments, an RF field of 250 kHz was used, resulting in ~17° degree tip angle for each nuclei, with recycle delays of 0.3 and 2.0 s. These conditions resulted in a semi-quantitative set of spectra. The Bruker three-pulse MQMAS experiment with a *z*-filter was used for the ^{27}Al MQMAS experiments (*mp3qzqf*). The RF field for the 3Q excitation pulse was 49 kHz, the 3Q conversion pulse was 208 kHz, and the central transition pulse was 13 kHz. A 20 μs *z*-filter delay was used with an initial t_1-period of 1 μs, and the phase-sensitive

Table 1 Fitting parameters of the ^{27}Al 1D MAS NMR data using the slices from the 3QMAS as a guide. In the tetrahedral sites, the peak at 60.2 ppm was fit using a Gaussian (G) type peak with a full-width half-max (FWHM) value of 1.96 ppm

Octahedral sites

Position (δ_{iso}, ppm)	Integrated Intensity (%)	C_Q (MHz)	η
4.5 ± 0.5	21.4 ± 1.7	4.5 ± 0.4	0.04 ± 0.01
6.2 ± 0.5	26.8 ± 2.2	6.2 ± 0.5	0.68 ± 0.06
5.8 ± 0.5	44.2 ± 3.6	10.6 ± 0.9	0.2 ± 0.02

Tetrahedral sites

Position (δ_{iso}, ppm)	Integrated Intensity (%)	C_Q (MHz)	η
67.8 ± 0.5	7.1 ± 0.6	4.1 ± 0.3	0.45 ± 0.04
		FWHM (ppm)	G/L
60.2 ± 0.5	0.5 ± 0.04	2.0 ± 0.2	G

States[34] acquisition mode was used. The resulting 2D data were sheared and processed using TopSpin® 3.2 (Bruker), where the shearing routine sets the anisotropic axis parallel with the F2 axis.

Uncertainties in the NMR parameters were estimated as follows: the overall fit from Dmfit was subtracted from the original spectrum. The absolute value of these residuals was then numerically integrated using Matlab and divided by the area under the original curve. This residual was 8.1% of the original spectrum, and that value was then used to estimate the error in the parameters of interest reported in Table 1, but not the peak positions, which are estimated to be certain to ±0.5 ppm.

Electronic structure methods

To compute the electric-field-gradient tensors (EFG), electronic-structure calculations at the density functional level of theory (DFT) were carried out using the Gaussian09 rev. E computational chemistry software package.[35] Protons were added by hand to the crystal structure of δ-Al$_{13}$ isomer as hydrogen atom locations were missing in the crystallographically determined structure. The H atom positions were optimized using the B3PW91/6-31+G* and PBE0/6-31+G* level of theory, while all other atom locations were fixed.[36–38] The B3PW91 functional was chosen due to its previous use on aluminum Keggin-isomers,[39] while the polarizability and diffusivity options in the basis set were chosen to allow for optimization of the isomer's geometry.[40] To assess the effect of counter ions on the EFG tensors, structures were optimized both with, and without, the sodium cap. The sodium-capped δ-Al$_{13}$ proved difficult to optimize in the gas phase, so instead the ion was modelled using a polarizable continuum model (PCM), which treats the ion as if it were in a solvated environment containing different layers of continuous dielectric medium.[41] The uncapped δ-Al$_{13}$ with a +7 charge could be optimized using PCM with both correlation and exchange functions. The EFG

calculations from these calculations were then executed at the same level of theory as the structure optimization. The EFG tensors were extracted from the output of the Gaussian calculation using EFGShield.[30]

Results

NMR

The ^{27}Al 1D MAS NMR spectra of the δ-Al$_{13}$ show peaks consistent with those published by Abeysinghe *et al.* (Fig. 2A), where characteristic peaks from the AlO$_4$ and AlO$_6$ sites of the Al$_{13}$-Keggin molecules are clear. The region where octahedral aluminum is typically found exhibits a broad resonance with a shoulder (+20 to −60 ppm). Some of this broadening is attributable to second-order quadrupolar effects. The tetrahedral site is clearly resolved with a maximum peak position of 64.5 ppm, but this peak displays second-order quadrupole broadening as well. The observed broadening for the tetrahedral peak in δ-Al$_{13}$ contrasts with spectra of ε-Al$_{13}$ where a single sharp peak at 62.5 ppm is observed due to the isotropic nature of its AlO$_4$ site. The site in the δ-Al$_{13}$ is distorted from high symmetry due to the displacement of the single trimeric cap. The 1D ^{23}Na MAS spectrum of the sample (Fig. 2B) exhibits two sites—a sharp peak at +6.2 ppm assignable to NaCl and a
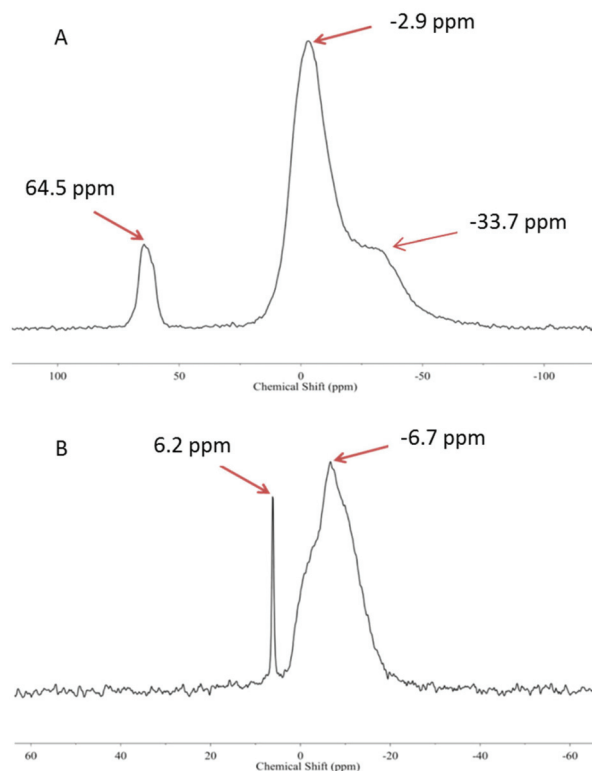
Fig. 2 (A) ^{27}Al MAS NMR spectrum of the δ-Al$_{13}$ isomer. Broad octahedral sites are seen between 20 and −60 ppm while a broad tetrahedral region is seen at 64.5 ppm. (B) ^{23}Na MAS NMR spectrum of the δ-Al$_{13}$ isomer, exhibit both free NaCl (6.2 ppm) and the capping sodium ion (−6.7 ppm).
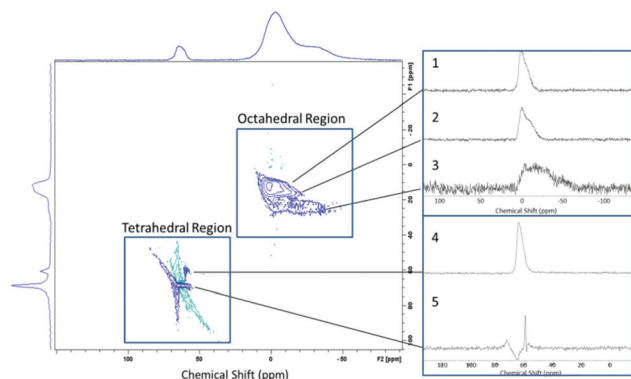
Fig. 3 ^{27}Al multiple-quantum MAS spectrum showing the isotropic projection on the F1 (left) axis while the ^{27}Al 1D MAS is projected along the F2 (top) axis. The two-dimensional set of FIDs has been sheared and processed to plot the anisotropic axis parallel to the F2 axis. Five distinct sites are seen, with three in the octahedral (20 to −60 ppm) region and two in the tetrahedral region (around 64.5 ppm). Slices from each isotropic site are shown on the right hand side of the figure.
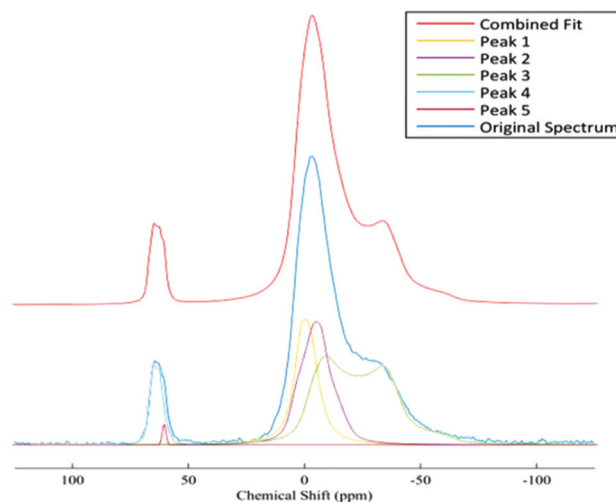

Fig. 4 Fit of the ^{27}Al 1D MAS spectrum of δ-Al$_{13}$ using the parameters estimated from quadrupolar lineshapes of the slices of the 3QMAS, showing five sites total (three in the octahedral region and two in the tetrahedral region).

broad peak centered between +3 and −20 ppm.[42,43] This broad peak is assigned to the sodium coordinated to the rotated trimeric cap of the δ-Al$_{13}$. The NaCl is a residual salt from the synthesis.

The broad resonances in the ^{27}Al spectrum for the δ-Al$_{13}$, in regions where the AlO$_4$ and AlO$_6$ coordination environments are typically found, cannot be unambiguously assigned to sites in the structure using 1D MAS. To accomplish these assignments, a ^{27}Al 3QMAS experiment was conducted. The contour peaks displayed in the 2D spectrum (Fig. 3) indicate correlation between the broad resonances in the 1D MAS spectrum (along the horizontal, or F2, axis) and the isotropic projections (along the vertical, or F1, axis). In this 3QMAS experiment, three distinct isotropic sites can be seen in the region of the spectrum where AlO$_6$ are typically assigned, and two distinct sites can be seen in the region of the spectrum typically assigned to AlO$_4$. From these data, slices were taken and fit using the analytical program DMFit.[44] The slices corresponding to individual isotropic sites were fit using either Gaussian or quadrupolar MAS lineshapes. The resulting spectral fits yielded estimates of the δ_{iso}, η, and C_Q parameters, which are reported in Table 1. The quality of the fits to the experimental linewidths can be seen in Fig. 4, where fits from individual sites overlay the experimental data and achieve the overall spectrum. The fits were approximately constrained to match the occupancy of the crystallographic sites (1 : 1 : 2 for AlO$_6$ sites).

EFG

The electronic-structure calculations for both exchange and correlation functionals to estimate the EFG tensors of the PCM embedded [δ-Al$_{13}$]$^{7+}$ resulted in the values for C_Q and η in Table 2. The individual aluminum sites are identifiable in Fig. 5.

After optimization in both calculations, there were five distinct types of aluminum in the δ-Al$_{13}$ structure. The tetrahedral

Table 2 EFG Calculations for the [δ-Al$_{13}$]$^{7+}$ in PCM at the B3PW91/6-31+G* level of theory (left) and for the PBE0/6-31+G* level of theory (right). Aluminum sites correspond to Fig. 5, where the tetrahedral aluminum (denoted Al$_{Td}$) was omitted for clarity

C_Q (MHz)	η		C_Q (MHz)	η
Rotated trimeric AlO$_6$, Al$_A$				
8.2	0.24	A$_1$	8.2	0.24
6.0	0.41	A$_2$	6.1	0.41
6.7	0.15	A$_3$	6.7	0.15
Bridging AlO$_6$, Al$_B$				
5.7	0.17	B$_1$	5.8	0.17
5.9	0.37	B$_2$	5.9	0.37
5.8	0.15	B$_3$	5.8	0.15
Unchanged AlO$_6$, Al$_C$				
9.8	0.01	C$_1$	9.8	0.00
8.2	0.30	C$_2$	8.3	0.30
8.8	0.18	C$_3$	8.9	0.18
9.9	0.19	C$_4$	10.0	0.19
9.5	0.25	C$_5$	9.5	0.25
10.4	0.17	C$_6$	10.5	0.18
AlO$_4$				
2.7	0.27	Al$_{Td}$	2.7	0.26
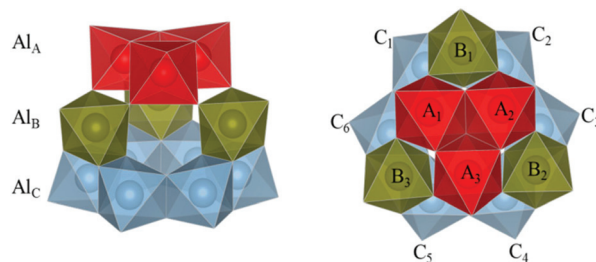
Fig. 5 Optimized structure for the δ-Al$_{13}$ isomer using B3PW91/6-31+G* level of theory. Aluminum species are color coded to show crystallographically distinct sites, and numbered to correspond to calculated quadrupolar parameters. The tetrahedral aluminum has been omitted for clarity.

AlO$_4$ site, identified as Al$_{Td}$, has the smallest C_Q, at 2.7 MHz. The remaining four types of aluminum correspond to different AlO$_6$ sites and have ranges of 5.7–6.1 MHz (A$_2$, B$_1$, B$_2$, B$_3$), 6.7 MHz (A$_3$), 8.2–8.3 MHz (A$_1$, C$_2$), and 8.9-10.5 MHz (C$_1$, C$_3$, C$_4$, C$_5$, C$_6$). If the anomalous 8.2 and 8.3 MHz sites are ignored, these values settle into two different sets of AlO$_6$ species, at around 6 MHz and 10 MHz.

Both sets of data show remarkable consistency, as the largest discrepancy between these two sets of calculations is 0.1 MHz.

Discussion

The results indicate a slight discrepancy between the measured C_Q and η values and those calculated *via* the electronic-structure methods. The values here measured for the δ-Al$_{13}$ isomer compare well with previous measurements for the other isomers,[23,24] a result that is expected due to the intermediate nature of the δ-Al$_{13}$ structure relative to the ε-Al$_{13}$ and γ-Al$_{13}$ structures. That three sets of AlO$_6$ sites are found in the NMR measurement is fully expected. Twist of the trimeric cap to corner-shared in the δ-Al$_{13}$ isomer from edge-shared in the ε-Al$_{13}$ isomer yields three crystallographically distinct AlO$_6$ sites (Fig. 5). While the AlO$_6$ site with the highest C_Q value and highest integrated intensity can be assigned to the Al$_C$ layer, the other two sites show remarkable similarity (δ_{iso} = 4.5 and 6.2 ppm) and cannot be unambiguously differentiated as either the Al$_A$ or Al$_B$ layers.

The more abundant edge-shared AlO$_6$ are similar in C_Q to those seen in the ε-isomer structure, which is an encouraging consistency. The AlO$_6$ from the rotated trimeric cap and the corner-shared AlO$_6$ also have C_Q similar to those seen in the γ-isomer structure, in that they are in the 4–6 MHz range, which is within error of the 6–7.5 MHz range seen in the γ-Al$_{13}$ values. These results can be rationalized by considering that the rotated trimer AlO$_6$ (Al$_A$) and the bridging AlO$_6$ units (Al$_B$) share a similar environment. Each AlO$_6$ in these sets is bound to two AlO$_6$ *via* a corner-shared linkage while also bound to two other AlO$_6$ *via* an edge-shared linkage. That these AlO$_6$ then would have similar C_Q values is unsurprising. The A and B sets of the AlO$_6$ are also identical in linkage to the AlO$_6$ seen in the γ-Al$_{13}$, so a similarity between the two is expected.

There is, however, still the discrepancy to address. Two calculated C_Q values differ distinctly from the other AlO$_6$ sites. Aluminums A$_1$ and C$_2$ have distinctly different C_Q values than those of the other A and C sets. It is possible that these sites are stabilized by the 2,6-NDS in the crystal lattice. Calculations to test this hypothesis have so far proved impossible because of the size of calculation.

A small gaussian-shaped signal is seen in the 3QMAS that is assignable to an unknown AlO$_4$ site. This peak cannot be due to an impurity from the ε-Al$_{13}$ because the δ_{iso} doesn't correspond to the expected 62.5 ppm. A tetrahedral site for aluminum with quadrupolar nature is also seen in the γ-Al$_{13}$ structure (measured at 1.75 MHz) while all calculations for the δ-Al$_{13}$ indicate an AlO$_4$ site with higher quadrupolar character than that AlO$_4$ site in the γ-Al$_{13}$ isomer (2.7 MHz in both calculations). This peak may correspond to a yet-undiscovered aluminum polyoxocation with a tetrahedral aluminum site.

Conclusions

The δ-Al$_{13}$-Keggin has been characterized using ^{27}Al and ^{23}Na 1D MAS NMR at high spinning speed and high field. Additionally, the structure was characterized using ^{27}Al MQMAS NMR. These experiments yielded information about the distinct AlO$_6$ sites within the δ-Al$_{13}$ structure and complement previous experiments for the ε-Al$_{13}$ and the γ-Al$_{13}$ structures. The experiments and calculations confirm the intermediate nature of AlO$_6$ sites within the δ-Al$_{13}$-Keggin structure, falling between those for the ε-Al$_{13}$ and γ-Al$_{13}$ isomers.

Acknowledgements

Notes and references

1 R. M. Garrels, F. T. MacKenzie and C. Hunt, *Chemical Cycles and the Global Environment*, Wm Kaufman Inc., Los Altos, 1975.

2 J. D. Hem, in *Kidney International*, ed. J. W. Cobum and A. C. Alfrey, Springer-Verlag, New York, 1986, pp. S3–S7.

3 J. J. Fitzgerald and A. H. Rosenberg, in *Antiperspirants and Deodorants*, ed. K. Laden, Marcel Dekker, New York, 2nd edn, 1999, pp. 83–136.

4 J. R. Sorenson, I. R. Campbell, L. B. Tepper and R. D. Lingg, *Environ. Health Perspect.*, 1974, **8**, 3–95.

5 G. Hass, *J. Opt. Soc. Am.*, 1949, **39**, 532.

6 C. Brosset, *Acta Chem. Scand.*, 1952, **6**, 910–940.

7 L. G. Sillen, *Acta Chem. Scand.*, 1954, **8**, 299–317.

8 G. Johansson, G. Lundgren, L. G. Sillen and R. Soderquist, *Acta Chem. Scand.*, 1960, **14**, 769–771.

9 L. F. Nazar, G. Fu and A. D. Bain, *J. Chem. Soc., Chem. Commun.*, 1992, 251–253.

10 D. K. Nordstrom and J. W. Ball, *Science*, 1986, **232**, 54–55.

11 K.-U. Ulrich and R. Pöthig, *Acta Hydrochim. Hydrobiol.*, 2000, **28**, 313–322.

12 G. Furrer, B. L. Phillips, K.-U. Ulrich, R. Pöthig and W. H. Casey, *Science*, 2002, **297**, 2245–2247.

13 Y. Kim, *Chemosphere*, 2015, **119**, 803–811.

14 J. F. Keggin, *Proc. R. Soc. London, Ser. A*, 1934, **144**, 75–100.

15 L. C. W. Baker and J. S. Figgis, *J. Am. Chem. Soc.*, 1970, **92**, 3794–3797.

16 L. Pauling, *Z. Kristallogr.*, 1933, **84**, 442–452.

17 W. B. Kamb, *Acta Crystallogr.*, 1960, **13**, 15–24.

18 G. Fu, L. F. Nazar and A. D. Bain, *Chem. Mater.*, 1991, **3**, 602–610.

19 J. Rowsell and L. F. Nazar, *J. Am. Chem. Soc.*, 2000, **122**, 3777–3778.

20 S. Abeysinghe, D. K. Unruh and T. Z. Forbes, *Cryst. Growth Des.*, 2012, **12**, 2044–2051.

21 S. E. Smart, J. Vaughn, I. Pappas and L. Pan, *Chem. Commun.*, 2013, **49**, 11352–11354.

22 J. F. Stebbins, S. Kroeker, S. Keun Lee and T. J. Kiczenski, *J. Non-Cryst. Solids*, 2000, **275**, 1–6.

23 L. Allouche, C. Huguenard and F. Taulelle, *J. Phys. Chem. Solids*, 2001, **62**, 1525–1531.

24 B. L. Phillips, C. A. Ohlin, J. Vaughn, W. Woerner, S. Smart, R. Subramanyam and L. Pan, *Inorg. Chem.*, 2016, **55**, 12270–12280.

25 L. Frydman and J. S. Harwood, *J. Am. Chem. Soc.*, 1995, 5367–5368.

26 A. Medek, J. S. Harwood and L. Frydman, *J. Am. Chem. Soc.*, 1995, **117**, 12779–12787.

27 J.-P. Amoureux and M. Pruski, in *Encyclopedia of Magnetic Resonance*, 2007, pp. 1–31.

28 J. Autschbach, in *Relativistic Methods for Chemists*, ed. M. Barysz and Y. Ishikawa, Springer, 2010, pp. 63–99.

29 H. Petrilli, P. Blöchl, P. Blaha and K. Schwarz, *Phys. Rev. B: Condens. Matter*, 1998, **57**, 14690–14697.

30 S. Adiga, D. Aebi and D. L. Bryce, *Can. J. Chem.*, 2007, **85**, 496–505.

31 A. C. Kunwar, A. R. Thompson, H. S. Gutowsky and E. Oldfield, *J. Magn. Reson.*, 1984, **60**, 467–472.

32 X. Guan and R. E. Stark, *Solid State Nucl. Magn. Reson.*, 2010, **38**, 74–76.

33 A. Detken, E. H. Hardy, M. Ernst and B. H. Meier, *Chem. Phys. Lett.*, 2002, **356**, 298–304.

34 D. J. States, R. A. Haberkorn and D. J. Ruben, *J. Magn. Reson.*, 1982, **48**, 286–292.

35 M. J. Frisch, G. W. Trucks, H. B. Schlegel, G. E. Scuseria, M. A. Robb, J. R. Cheeseman, G. Scalmani, V. Barone, G. A. Petersson, H. Nakatsuji, X. Li, M. Caricato, A. Marenich, J. Bloino, B. G. Janesko, R. Gomperts, B. Mennucci, H. P. Hratchian, J. V. Ortiz, A. F. Izmaylov, J. L. Sonnenberg, D. Williams-Young, F. Ding, F. Lipparini, F. Egidi, J. Goings, B. Peng, A. Petrone, T. Henderson, D. Ranasinghe, V. G. Zakrzewski, J. Gao, N. Rega, G. Zheng, W. Liang, M. Hada, M. Ehara, K. Toyota, R. Fukuda, J. Hasegawa, M. Ishida, T. Nakajima, Y. Honda, O. Kitao, H. Nakai, T. Vreven, K. Throssell, J. A. Montgomery, Jr., J. E. Peralta, F. Ogliaro, M. Bearpark, J. J. Heyd, E. Brothers, K. N. Kudin, V. N. Staroverov, T. Keith, R. Kobayashi, J. Normand, K. Raghavachari, A. Rendell, J. C. Burant, S. S. Iyengar, J. Tomasi, M. Cossi, J. M. Millam, M. Klene, C. Adamo, R. Cammi, J. W. Ochterski, R. L. Martin, K. Morokuma, O. Farkas, J. B. Foresman and D. J. Fox, *Gaussian 09, Revision E.01*, Gaussian, Inc., Wallingford CT, 2016.

36 A. D. Becke, *J. Chem. Phys.*, 1993, **98**, 5648–5652.

37 J. P. Perdew and Y. Wang, *Phys. Rev. B: Condens. Matter*, 1992, **45**, 13244–13249.

38 J. P. Perdew, M. Ernzerhof and K. Burke, *J. Chem. Phys.*, 1996, **105**, 9982–9985.

39 C. A. Ohlin, J. R. Rustad and W. H. Casey, *Dalton Trans.*, 2014, **43**, 14533–14536.

40 D. Young, *Computational Chemistry: A Practical Guide for Applying Techniques to Real World Problems*, Wiley and Sons, 2001.

41 E. Cancès, B. Mennucci and J. Tomasi, *J. Chem. Phys.*, 1997, **107**, 3032.

42 S. E. Ashbrook, L. Le Pollès, R. Gautier, C. J. Pickard and R. I. Walton, *Phys. Chem. Chem. Phys.*, 2006, **8**, 3423–31.

43 Y. Kim and R. J. Kirkpatrick, *Geochim. Cosmochim. Acta*, 1997, **61**, 5199–5208.

44 D. Massiot, F. Fayon, M. Capron, I. King, S. Le Calvé, B. Alonso, J.-O. Durand, B. Bujoli, Z. Gan and G. Hoatson, *Magn. Reson. Chem.*, 2002, **40**, 70–76.

45 K. Momma and F. Izumi, *J. Appl. Crystallogr.*, 2011, **44**, 1272–1276.